

# Kinematics Analysis of a Hybrid Robot Consisting of a SCARA and a Parallel Wrist

Feng Liang, Guoying Zhang, Tao Zhang\*, Yisheng Guan\* and Guanfeng Liu

*Biomimetic and Intelligent Robotics Lab (BIRL)*

*School of Electromechanical Engineering*

*Guangdong University of Technology, Guangzhou, China, 510006*

**Abstract**—For some manipulation tasks needing to change objects' orientation and position quickly, a hybrid robot, consisting of a 4-DOFs SCARA and a 3-DOFs (2R1T) parallel wrist, is presented. First, the swing and translation characteristics of the parallel wrist are quantitatively analyzed by numerical method, and its maximum swing angle and optimum working curve are obtained. A swing-rotation method for representing the attitude of the parallel wrist is proposed, and it can be transformed with the commonly used Azimuth-Swing method, which is the key to decouple kinematics of hybrid robots. Then, the singularity of the mechanism, when its attitude expressed by the proposed method, is also analyzed. The forward and inverse kinematic equations are derived in an analytical form. Finally, the kinematics simulation based on ADAMS verifies the correctness of the robot kinematics.

**Index Terms**—Hybrid Robot, Parallel Wrist, Kinematics

## I. INTRODUCTION

SCARA is widely used in plastic, automobile, electronic products, pharmaceutical and food industry. However, many manipulation tasks in industrial applications can not be accomplished by manipulators with less than 6-DOFs. Recently, we developed a parallel wrist, as shown in Fig. 1(a), which has a symmetrical three revolute-spherical-revolute (3-RSR) configuration [1], [2]. The parallel mechanism consists of a moving platform, a base and three identical branches. The moving platform and the base have equal radius. These chains are uniformly distributed between the base and the moving platform at 120 degrees, as shown in Fig. 1(c), and connect with the base and the moving platform by rotating pairs. The axes of the rotating pairs linking to the base or the moving platform intersect at their central points. The connection between the spherical pair center and the base center in each branch chain is perpendicular to the axis of the driving pair, and the connection between the spherical pair center and the moving platform center is always perpendicular to the axis of the rotating pair connected with it. The plane, defined by

\*Corresponding author: tzhang@gdut.edu.cn ysguan@gdut.edu.cn. The work in this paper is partially supported by the National Natural Science Foundation of China (Grant No. 51905105), the Natural Science Foundation of Guangdong Province (Grant No. 2015A030308011), and the Frontier and Key Technology Innovation Special Funds of Guangdong Province (Grant No. 2017B050506008, 2017B090910008).

the center of the three spherical pairs, is a middle symmetric plane [3]. During the movement, the moving platform and the base are always symmetrical with the middle symmetric plane. This special spatial layout and symmetry facilitates the equivalent simplification and kinematics analysis of the mechanism. The DOF of this mechanism is analyzed in [3].

For some manipulation tasks that need to quickly change objects' orientation and position, the parallel wrist is installed at the end of SCARA as an end effector to form a hybrid robot, which has 7 DOFs. The hybrid robot takes full advantage of SCARA's wide working range, fast positioning and Parallel Wrist's swing performance, and is suitable for some 3C assembly scenarios.

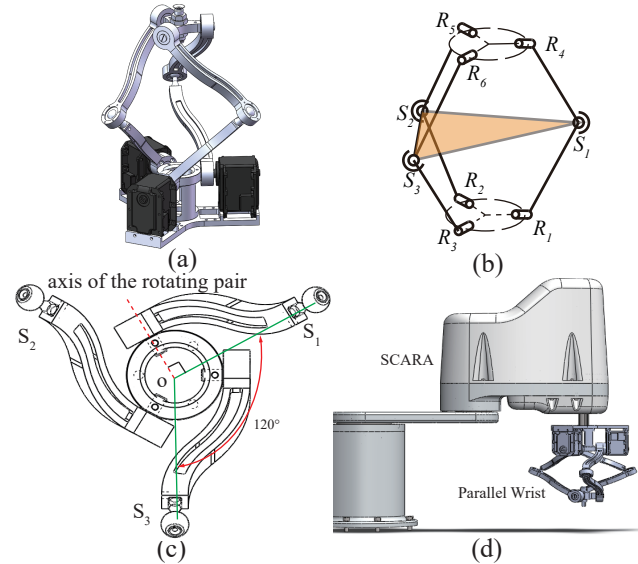


Fig. 1. Overview of the hybrid robot. (a) Parallel Wrist. (b) Schematic Diagram of the Parallel Wrist. (c) Spatial Distribution of the Parallel Wrist Structure. (d) 3D model of the Hybrid Robot.

This paper presents the kinematic performance analysis of the parallel wrist. Besides, a new method to depict the wrist posture is proposed, which is the key to decouple kinematics of the hybrid robot. Moreover, the equivalent kinematics model of the robot is established, and the forward and inverse kinematics equations in analytical form are deduced. Finally,

the kinematics simulation based on ADAMS verifies the correctness of the kinematics equations.

## II. PERFORMANCE ANALYSIS AND POSTURE REPRESENTATION OF THE PARALLEL WRIST

### A. Performance Analysis

As we can see in Fig. 2(a), the angle between the X direction of the base coordinate system and the connection between the base center and the foot of perpendicular, which is projected by the moving platform center to the X-Y plane of the base, is defined as azimuth angle:  $\alpha$ . The angle between the normal direction of moving platform and the normal direction of base is defined as swing angle  $\beta$ . The attitude of the parallel wrist can be described by this two angle: azimuth and swing angles. Without changing the attitude, the mechanism can move along the normal direction of the moving platform [3]. There are two important indexes for the mechanism performance: swing performance and translation performance, which are characterized by the swing angle that can be reached by the mechanism and described by the distance between the moving platform center and the base center, respectively.

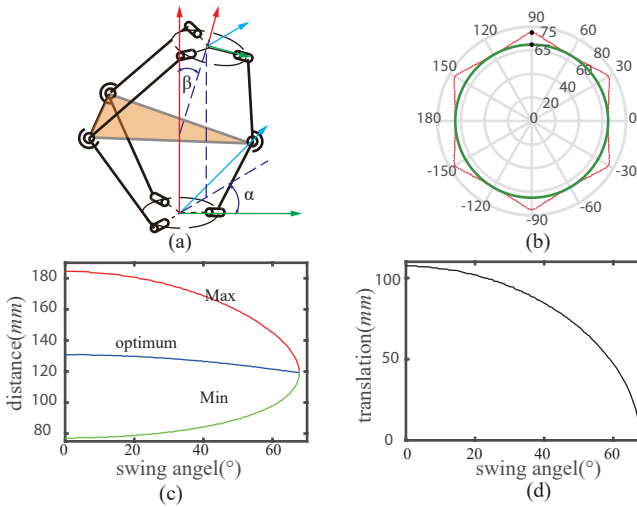


Fig. 2. Performance analysis of the Parallel Wrist. (a) Posture Representation. (b) Swing performance. (c) Center distance versus swing angle. (d) Translation versus swing angle.

1) *Swing Performance Analysis:* From the polar coordinate in Fig. 2(b), the swing performance of the mechanism is central symmetry. In the whole cycle, the maximum swing angle is  $60^\circ$ . But in some azimuths, such as  $\alpha = 30^\circ$ , the maximum swing angle is  $75^\circ$ .

2) *Translation Performance Analysis:* At a specific azimuth angle, the maximum distance between the moving platform center and the base center decreases with the increase of the swing angle, as shown in Fig. 2(C). Meanwhile, the minimum distance between the moving platform center and the base center increases with the increase of the swing

angle. Taking the average of the maximum and the minimum distances to get the middle curve, which can be considered as the best motion curve of parallel wrist. It can be seen from Fig. 2 (d) that the translation performance of the mechanism decreases with the increase of the swing angle.

### B. Posture Representation

Usually, the attitude of this kind of mechanism, which has 2 rotational DOFs, is described by azimuth and swing angles. However, the parallel wrist is installed at the end of SCARAs. The rotation of the fourth axis of SCARA changes the azimuth angle of the whole wrist. The wrist itself also has an azimuth angle. These two azimuths angle are repeated. Therefore, the DOFs of the hybrid robot are reduced to five operational DOFs plus two redundant DOFs. In order to realize the kinematic decoupling of the robot with six operational DOFs, the wrist posture expression method must be changed. This paper presents a new description method: the swing-rotation angle method.

1) *Swing-Rotation Angle Method:* When the azimuth is zero, Given a specific swing angle, the attitude coordinate of the moving platform can be presented as coordinate system (1) in Fig. 3(a). When the swing angle is kept unchanged and the azimuth angle is changed to  $\alpha$ , the attitude coordinate of the moving platform changes to coordinate system (2). The coordinate system (3) is obtained by rotating coordinate system (1) around the normal direction of the base. The rotation angle of the X-axis of coordinate system (2) relative to the X-axis of coordinate system (3) is defined as the wrist rotation angle:  $\gamma$ . Obviously, the wrist rotation angle is related to its azimuth angle. Given several swing angles, the rotation angles corresponding to different azimuths are calculated respectively, and the results are drawn as Fig. 3(b). When the swing angle  $\beta = 65^\circ$ , there are many intersections between the azimuth-turning curve and the dotted line in the graph, which indicates that the same rotation angle corresponds to multiple azimuth angle. When the swing angle  $\beta \leq 60^\circ$ , the rotation angle and azimuth angle are one to one correspondence. Therefore, the azimuth-swing angle method and the swing-rotation angle method can transform to each other.

2) *Relationship between Rotation Angle and Azimuth Angle:* Given several swing angles, the difference between rotation angle and azimuth angle versus azimuth angle is plotted in Fig. 3(c). Because  $\alpha \in [-180^\circ, 0^\circ]$  and  $\alpha \in [0^\circ, 180^\circ]$  has the same law of change, So we just take a period to study. There are several special positions:  $\alpha = -180^\circ$ ,  $\alpha = -90^\circ$ ,  $\alpha = 0^\circ$ ,  $\alpha = 90^\circ$  or  $\alpha = 180^\circ$ , the rotation angles is the same as the azimuth angle. When the swing angle is different, the maximum difference between the rotation and azimuth angle is calculated and plotted in Fig. 3(d). The relationship between the swing angle and the maximum difference is solved by function fitting method [4], and we can

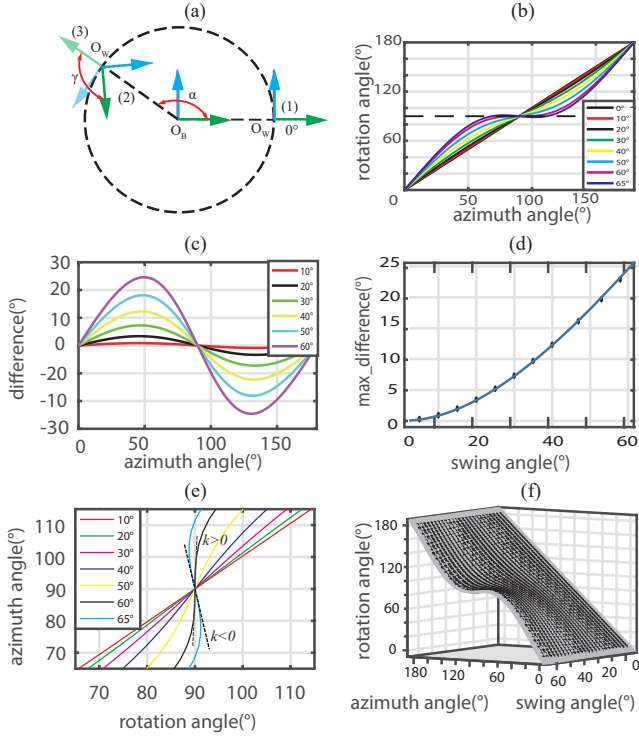


Fig. 3. Posture representation method. (a) Rotation angle definition. (b) Rotation angle versus azimuth angle at different swing angles. (c) (Rotation angle - azimuth) versus azimuth angle at different swing angles. (d) Maximum(rotation angle - azimuth angle) versus swing angle. (e) At special positions, azimuth angle versus rotation angle varies at different swing angles. (f) Azimuth angle, swing angle and rotation angle are depicted as three-dimensional surface.

get:  $differ_{max} = f_d(\beta) = k_1 + k_2 \cos(\beta\omega) + k_3 \sin(\beta\omega) + k_4 \cos(2\beta\omega) + k_5 \sin(2\beta\omega)$ , where  $k_1 = 54.02$ ,  $k_2 = -53.32$ ,  $k_3 = -12.04$ ,  $k_4 = -0.6695$ ,  $k_5 = 5.766$ ,  $\omega = 0.01853$ . When  $\gamma \in (0, 90)$  or  $\gamma \in (-180, -90)$ ,  $\alpha \in [\gamma - f_a(\beta), \gamma]$ . When  $\gamma \in (90, 180)$  or  $\gamma \in (-90, 0)$ ,  $\alpha \in [\gamma, \gamma + f_a(\beta)]$ . The interval of  $\alpha$  is known, so it can be solved by dichotomy method[5]. The calculation process is shown in Fig. 4. In this way, when the wrist rotation and swing angle are known, the corresponding azimuth angle can be solved, and then the inverse solution can be obtained by the original method, which will be discussed in the later section.

3) Singularity analysis: The relationship between rotation angle and azimuth angle at special positions (When  $\gamma$  is near  $90^\circ$ ) is analyzed. In Fig. 3(e), when  $\beta = 60^\circ$ , the slope at curve crossing point  $(90^\circ, 90^\circ)$  is greater than zero, meanwhile, when  $\beta = 65^\circ$ , the slope at curve crossing point  $(90^\circ, 90^\circ)$  is less than zero. There must be  $\beta \in (60^\circ, 65^\circ)$  with infinite slope at the curve crossing point  $(90^\circ, 90^\circ)$ . At this point, the mechanism is singular, and the swing angle at this time is called critical swing angle. When the swing angle is less than the critical swing angle, the larger the swing angle is, the greater the slope at the curve crossing point  $(90^\circ, 90^\circ)$ . That is to say, the faster the azimuth angle changes, the worse

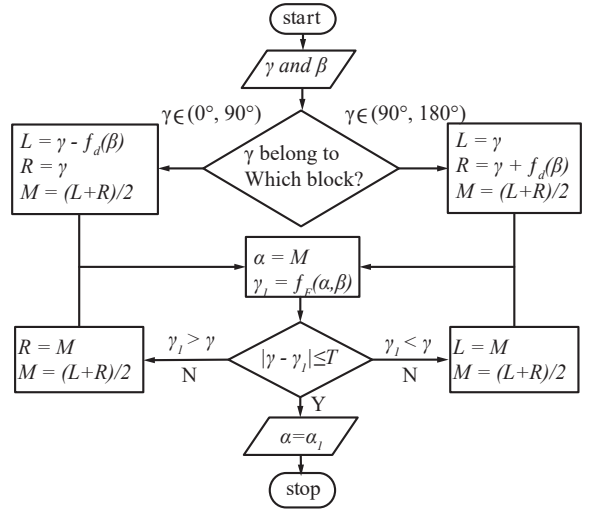


Fig. 4. Solving Azimuth Angle.

the operational performance of the mechanism will be. When the swing angle exceeds the critical swing angle, the same rotation angle corresponds to multiple azimuth angles, and the mechanism is inoperable.

### III. KINEMATIC ANALYSIS

SCARA and parallel wrist are connected in series. The forward kinematics solutions of SCARA and parallel wrist can be solved respectively, and then the two parts can be combined to form the forward kinematics solution of hybrid robot.

#### A. Forward Kinematics

1) Forward Kinematics of SCARA: Based on D-H method [6], the coordinate system of SCARA is established, as shown in Fig. 5. The parameters of SCARA's Links are drawn into Table 1. The transformation matrix of the end coordinate system 4 relative to the base coordinate system 0 can be obtained:

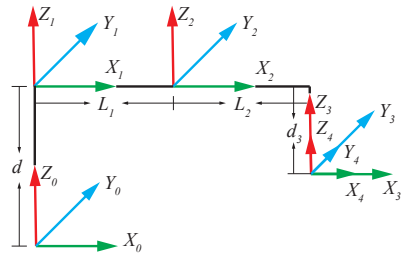


Fig. 5. Coordinate System of SCARA.

$$T_s = \begin{bmatrix} c(\theta_1+\theta_2+\theta_4) & -s(\theta_1+\theta_2+\theta_4) & 0 & L_2c(\theta_1+\theta_2)+L_1c\theta_1 \\ s(\theta_1+\theta_2+\theta_4) & c(\theta_1+\theta_2+\theta_4) & 0 & L_2s(\theta_1+\theta_2)+L_1s\theta_1 \\ 0 & 0 & 1 & d-d_3 \\ 0 & 0 & 0 & 1 \end{bmatrix} \quad (1)$$

TABLE I  
SPECIFICATIONS OF FOUR JOINT MODULES.

Joints	$a_{i-1}$	$\alpha_{i-1}$	$d_i$	$\theta_i$
1	0	0	$d$	$\theta_1$
2	$L_1$	0	0	$\theta_2$
3	$L_2$	0	$d_3$	0
4	0	0	0	$\theta_4$

2) *Forward Kinematic of Parallel Wrist:* Firstly, the coordinate system is established on the base of parallel wrist, as show in Fig. 6. The origin of the coordinate system is the center of the base. Axis X coincides with the axis of the rotating pair  $R_1$ . Axis Z is the normal direction of the base. Axis Y is obtained by the cross product of axis Z with axis X. The position of the ball pair can be expressed as:

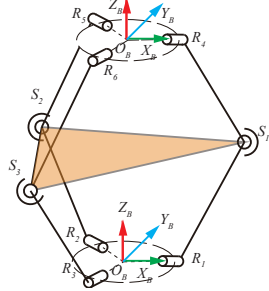


Fig. 6. Coordinate System of Parallel Wrist.

$$\vec{O_B S_i} = T_i [0 \ L c\phi_i \ L s\phi_i] \quad (i = 1, 2, 3) \quad (2)$$

where  $T_i = \begin{bmatrix} c\alpha_i & -s\alpha_i & 0 \\ s\alpha_i & c\alpha_i & 0 \\ 0 & 0 & 1 \end{bmatrix}$ ,  $\alpha_i = \frac{2(i-1)\pi}{3}$ ,  $L$  means the length of the parallel wrist link, and  $\phi_i$  means the swing angle of the  $i$ -th active link. There are two vectors in the plane  $S_1 S_2 S_3$ :  $\vec{S_1 S_2} = \vec{O_B S_2} - \vec{O_B S_1}$  and  $\vec{S_1 S_3} = \vec{O_B S_3} - \vec{O_B S_1}$ . Therefore, we can solve the directional vector of the plane and unify its directional vector:  $\vec{N} = \vec{S_1 S_2} \times \vec{S_1 S_3}$ , and  $\vec{n} = \frac{\vec{N}}{\|\vec{N}\|}$ . Because point  $O_B$  and point  $O_W$  are symmetric with plane  $S_1 S_2 S_3$ , then we can get:

$$\vec{O_B O_W} = 2(\vec{n} \cdot \vec{O_B S_1})\vec{n} = (X_w, Y_w, Z_w) \quad (3)$$

$$\vec{O_B R_i} = T_i [R \ 0 \ 0] \quad (i = 1, 2, 3) \quad (4)$$

In the plane of  $O_B R_1 S_1$ ,  $\vec{R_1 S_1} = \vec{O_B S_1} - \vec{O_B R_1}$ . Because point  $R_1$  and point  $R_4$  are symmetric about plane  $S_1 S_2 S_3$ , thus we get:

$$\vec{R_1 R_4} = 2(\vec{n} \cdot \vec{R_1 S_1})\vec{n} \quad (5)$$

In the plane of  $O_B R_1 R_4$ ,  $\vec{O_B R_4} = \vec{O_B R_1} + \vec{R_1 R_4}$ . In the plane of  $O_B O_W R_4$ ,  $\vec{O_W R_4} = \vec{O_B R_4} - \vec{O_B O_W}$ . Similarly, vector  $\vec{O_W R_5}$  can be solved. The coordinate system on the moving platform can be solved:  $\vec{W_x} = \frac{\vec{O_W R_4}}{\|\vec{O_W R_4}\|}$ ,  $\vec{W_z} = \frac{\vec{O_W R_4} \times \vec{O_W R_5}}{\|\vec{O_W R_4} \times \vec{O_W R_5}\|}$ ,

$\vec{W_y} = \frac{\vec{W_z} \times \vec{W_x}}{\|\vec{W_z} \times \vec{W_x}\|}$ . The position and posture of the parallel wrist can be expressed in matrix form:

$$T_w = \begin{bmatrix} W_x(1) & W_y(1) & W_z(1) & X_w \\ W_x(2) & W_y(2) & W_z(2) & Y_w \\ W_x(3) & W_y(3) & W_z(3) & Z_w \\ 0 & 0 & 0 & 1 \end{bmatrix} \quad (6)$$

3) *Forward Kinematics of Hybrid Robot:* Establishing the coordinate system of the hybrid robot as Fig. 7. We can easily get the forward kinematics of the hybrid robot as:

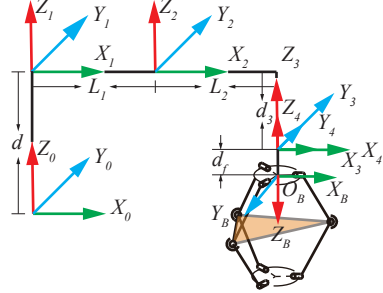


Fig. 7. Coordinate System of Hybrid Robot.

$$T_c = \begin{bmatrix} 1 & 0 & 0 & 0 \\ 0 & -1 & 0 & 0 \\ 0 & 0 & -1 & -d_f \\ 0 & 0 & 0 & 1 \end{bmatrix} \quad (7)$$

$$T = T_s T_c T_w \quad (8)$$

### B. Inverse Kinematic

According to previous analysis, the posture of parallel wrist can be expressed by swing angle and rotation angle. The rotation of the fourth axis of SCARA changes the azimuth angle of the whole parallel wrist. Thus, the posture of hybrid robot is determined by the parallel wrist and the fourth axis. The parallel wrist provides the swing and rotation movements of the robot, and the fourth axis provides the azimuth movement. The end position of the hybrid robot is determined by the first three axes. The kinematics of a hybrid robot can be decoupled. In other words, its position and posture can be independently controlled.

1) *Inverse Kinematics of Hybrid Robot:* For grabbing task, given the orientation vector and the corresponding rotation angle:  $\gamma$  of the working face. The position  $[X, Y, Z]$  of the grabbing point is also given. The orientation vector can be decomposed into azimuth angle  $\alpha$  and swing angle  $\beta$ . The process of solving inverse kinematics of the robot is shown in the Fig. 8. Using the previous method, when the swing angle  $\beta$  and the rotation angle  $\gamma$  of parallel wrist is known, the corresponding azimuth angle can be calculated to be  $\alpha_1$ . The relationship between posture and position of parallel wrists is as follows:

$$\begin{cases} X_w = L_{BW} \sin \frac{\beta}{2} \cos \alpha_1 \\ Y_w = L_{BW} \sin \frac{\beta}{2} \sin \alpha_1 \\ Z_w = L_{BW} \cos \frac{\beta}{2} \end{cases} \quad (9)$$

In the Fig. 8,  $\vec{O_4O_W} = \vec{O_4O_B} + R \cdot \vec{O_BO_W}$ ,  $\vec{O_0O_4} = \vec{O_0O_W} - R_s \cdot \vec{O_4O_W}$ , and  $[X_s, Y_s, Z_s] = \vec{O_0O_4}$ , where:

$$R = \begin{bmatrix} W_x(1) & -W_y(1) & -W_z(1) \\ W_x(2) & -W_y(2) & -W_z(2) \\ W_x(3) & -W_y(3) & -W_z(3) \end{bmatrix} \quad (10)$$

$$R_s = \begin{bmatrix} c(\alpha - \alpha_1) & -s(\alpha - \alpha_1) & 0 \\ s(\alpha - \alpha_1) & c(\alpha - \alpha_1) & 0 \\ 0 & 0 & 1 \end{bmatrix} \quad (11)$$

Next, we explain how to solve the inverse kinematics of SCARA and parallel wrist respectively.

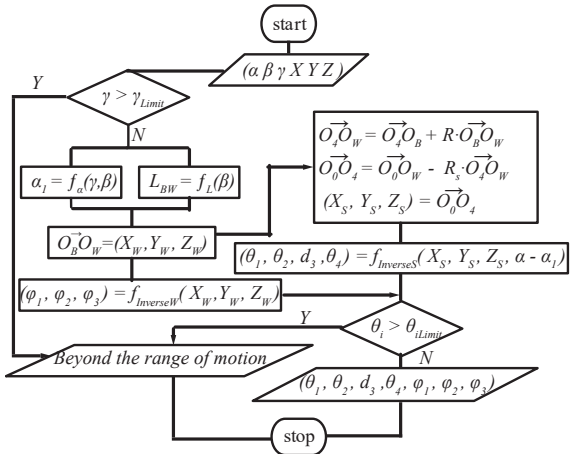


Fig. 8. Hybrid Robot Inverse.

2) *Inverse Kinematic of Parallel Wrist:* The inverse solution of parallel mechanism can be solved by geometric method. The link length of parallel wrists is known as  $L$ , therefore  $\|O_B^-S_i\| = L$ ,  $i = (1, 2, 3)$ .  $O_B^-O_W \perp plane S_1S_2S_3$ .  $O_B^-S_1 \cdot O_B^-O_W = \frac{1}{2}L_{BW}$ . Because of the special position of the mechanism coordinate system, the following relations exist:  $S_1(x) = 0$ ,  $S_2(x) - \sqrt{S_2(y)} = 0$ , and  $S_3(x) + \sqrt{S_3(y)} = 0$ . There are 9 unknown parameters and 9 equations at the same time, hence  $S_1(x)$ ,  $S_1(y)$ ,  $S_1(z)$ ,  $S_2(x)$ ,  $S_2(y)$ ,  $S_2(z)$ ,  $S_3(x)$ ,  $S_3(y)$  and  $S_3(z)$  can be solved:

$$\left\{ \begin{array}{l} \phi_1 = \arctan \frac{S_1(z)}{\sqrt{S_1(x)^2 + S_1(y)^2}} \\ \phi_2 = \arctan \frac{S_2(z)}{\sqrt{S_2(x)^2 + S_2(y)^2}} \\ \phi_3 = \arctan \frac{S_3(z)}{\sqrt{S_3(x)^2 + S_3(y)^2}} \end{array} \right. \quad (12)$$

3) *Inverse Kinematics of SCARA:* Closed kinematics solutions of manipulators can be obtained in two ways: algebraic method and geometric method. Geometric method is used to solve the inverse kinematics of SCARA in this paper. Considering the first and second joints, the robot is simplified to a planar 2-DOFs manipulator, as shown in the Fig. 9. When  $X_s \neq 0$ :  $\phi_1 = \arctan \frac{Y_s}{X_s}$ . Otherwise, when  $X_s = 0, Y_s > 0$ :  $\phi_1 = 90^\circ$  and  $X_s = 0, Y_s < 0$ :  $\phi_1 = -90^\circ$ . In addition,  $X_s$  and  $Y_s$  will not be zero at the same time. Because  $L_1 = L_2$ ,

$\triangle O_0O_2O_4$  is an isosceles triangle,  $\phi_2 = \arccos \frac{\sqrt{X_s^2 + Y_s^2}}{2L_1}$ , ( $0 \leq \phi_2 \leq 90^\circ$ ). Then, the rotation angles of the first and second joints of SCARA can be obtained.  $\theta_1$  and  $\theta_2$  are both has two solutions, then it is necessary to select which is the better one. The weight of the end joint is light and its inertia is small, while the mass of the base part of the robot is heavy and its inertia is large. Also the load of the end part acts on the first joint. From the view point of minimizing energy loss [7], it should minimize the movement of the first joint. When  $\theta_1$  is selected,  $\theta_2$  will be uniquely determined. The translation of the third joint is easy to solve:  $d_3 = d - Z_s$ . The posture of SCARA is superposed by the first, second and fourth joints, and it should be the azimuth angle of the hybrid robot minus the azimuth angle of the parallel wrist:  $\theta_1 + \theta_2 + \theta_4 = \alpha - \alpha_1$ . Thus,  $\theta_4 = \alpha - \alpha_1 - \theta_1 - \theta_2$  and:

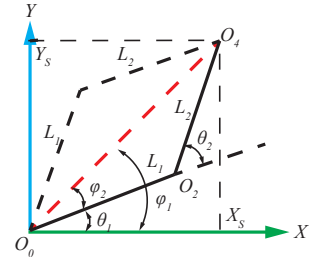


Fig. 9. Inverse kinematics of SCARA.

$$\left\{ \begin{array}{l} \theta_1 = \phi_1 + \phi_2 = \arctan \frac{Y_s}{X_s} \pm \arccos \frac{\sqrt{X_s^2 + Y_s^2}}{2L_1} \\ \theta_2 = \pm 2\phi_2 = \pm 2\arccos \frac{\sqrt{X_s^2 + Y_s^2}}{2L_1} \end{array} \right. \quad (13)$$

#### IV. KINEMATIC SIMULATION

In order to verify the correctness of kinematics, a simulation based on ADAMS [8] is carried out. Assuming the working path of the robot is an arc, as shown in the Fig. 11. The starting point, middle point and end point of the arc are A, B and C, respectively. The positions and postures of robots at points A, B and C are  $P_1(250, -200, -63.5898, 90^\circ, 30^\circ, -180^\circ)$ ,  $P_2(250, 0, -10, 0^\circ, 0^\circ, 0^\circ)$  and  $P_3(250, 200, -63.5898, -90^\circ, 30^\circ, 180^\circ)$ , respectively. A series of interpolation points are obtained by Cartesian space trajectory planning method [9], [10], [11]. By substituting each interpolation point into the inverse kinematics of the robot, the corresponding variables of each joint can be obtained, as shown in the Fig. 11. The kinematics simulation environment of the robot is established in ADAMS. The variables of each joint are used as simulation input to get the position of the end effector. As shown in the Fig. 10, the end effector of the robot moves from point A to point C. At the same time, the position of the end effector can also be obtained by taking the variables of each joint as the input of the forward kinematics solution. The calculated values are compared with the simulation values, and the results are shown in the Fig. 11. It can be

seen from the figure that the calculated value is in good agreement with the simulation value. It shows that the forward and inverse kinematics of the robot are correct.

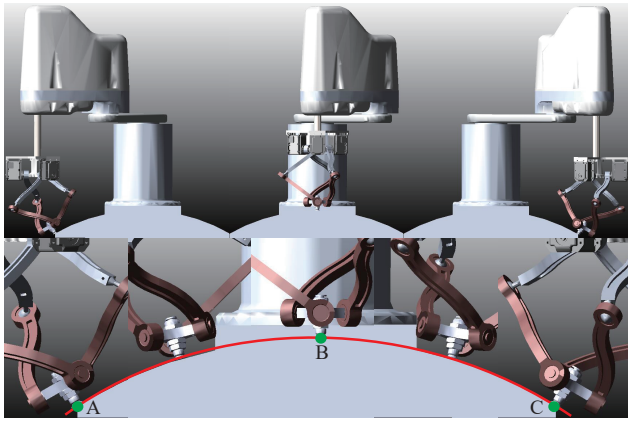


Fig. 10. Kinematic Simulation Base on ADAMS.

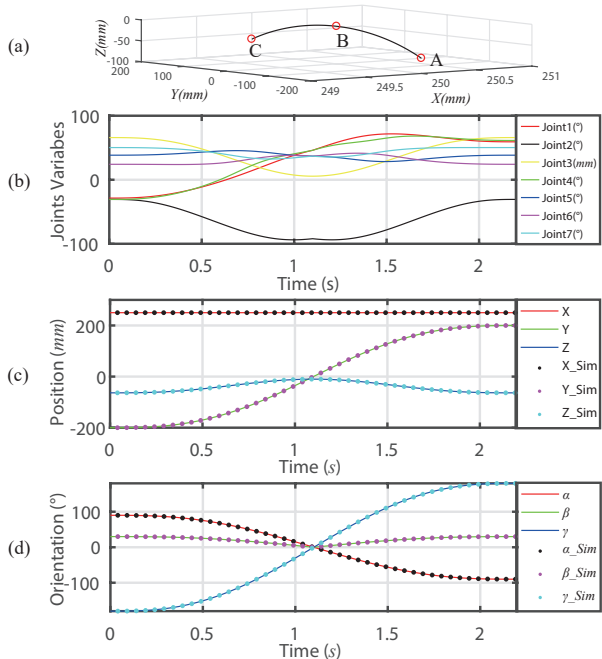


Fig. 11. (a) Working Path of the robot. (b) Joint Variables Corresponding to Interpolation Points. (c) Comparisons between Simulation Results and Calculation Results of End-effector Position. (d) Comparisons between Simulation Results and Calculation Results of End-effector Orientation

## V. CONCLUSION

A Hybrid robot consists of a 4-DOFs SCARA and a 3-DOFs (2R1T) parallel wrist is presented in this paper. Firstly, the swing and translation characteristics of the parallel wrist are analyzed, and the maximum swing angle in the whole circle and the optimal working curve of the mechanism are

obtained. A new method (Swing-Rotation method) is proposed to represent the attitude of the mechanism that makes the kinematics of the robot decoupled. The singularity of the mechanism is also analyzed. Then, the forward and inverse kinematics of the robot is deduced. Finally, the kinematics simulation based on ADAMS verifies the correctness of the forward and inverse kinematics of the robot and simulates the working scene of the robot.

## REFERENCES

- [1] R. D. Gregorio, "Kinematics of the 3-rsr wrist," *Robotics IEEE Transactions on*, vol. 20, no. 4, pp. 750–753, 2004.
- [2] Z. Bing, F. Hao, R. Lu, and Z. Feng, "Closed-form direct position kinematics solution for a 3-rsr platform manipulator," in *World Congress on Intelligent Control & Automation*, 2000.
- [3] G. Zhang, Y. Liao, F. Liang, M. Su, Y. Guan, G. Liu, and X. Chen, "A spheroid parallel wrist mechanism and its kinematic analysis," *Robot*, vol. 39, no. 2, pp. 167–175, 2017.
- [4] G. Chen, Z. L. Ren, and H. Z. Sun, "Curve fitting in least-square method and its realization with matlab," *Ordnance Industry Automation*, 2005.
- [5] Y. Chen, X. P. Yu, and J. Z. Xiong, "Approximation accuracies of a class of polynomial smoothing functions," *Journal of Computer Applications*, vol. 30, no. 8, pp. 2041–2044, 2010.
- [6] J. J. Craig, *Introduction to Robotics: Mechanics and Control*, 1955.
- [7] V. Spanier, "Optimized scara kinematic, description and examples," in *Robotics*, 2011.
- [8] F. Cheraghpour, M. Vaezi, H. E. S. Jazeh, and S. A. A. Moosavian, "Dynamic modeling and kinematic simulation of stubli tx40 robot using matlab/adams co-simulation," in *IEEE International Conference on Mechatronics*, 2011.
- [9] C. Melchiorri, *Trajectory Planning for Automatic Machines and Robots*, 2009.
- [10] C. G. Mohr and R. L. Vaughan, "An economical procedure for cartesian interpolation and display of reflectivity factor data in three-dimensional space," *Journal of Applied Meteorology*, vol. 18, no. 5, pp. 661–670, 1979.
- [11] L. I. Li, J. Shang, Y. Feng, and H. Yawen, "Research of trajectory planning for articulated industrial robot - a review," *Computer Engineering & Applications*, 2018.